analytical chemistry

Article

pubs.acs.org/ac

Microfluidic Chemical Function Generator for Probing Dynamic Cell Signaling

Peng Chen,[†] Yiran Guo,[†] Xiaojun Feng, Shuangqian Yan, Jie Wang, Yiwei Li, Wei Du, and Bi-Feng Liu*

The Key Laboratory for Biomedical Photonics of MOE at Wuhan National Laboratory for Optoelectronics−Hubei Bioinformatics & Molecular Imaging Key Laboratory, Systems Biology Theme, Department of Biomedical Engineering, College of Life Science and Technology, Huazhong University of Science and Technology, Wuhan 430074, China

Supporting Information

ABSTRACT: Cellular environments are inherently dynamic and generally involve complex, temporally varying signals. Reconstruction of these environments with high spatial and temporal fidelity and simultaneous imaging of intracellular dynamics in live cells remains a major challenge. In this paper, a microfluidic chemical function generator (μCFG) was proposed for probing cell dynamic signaling with high temporal resolution. By combining a hydrodynamic gating module with a chaotic advection mixing module, the μCFG was able to generate a variety of chemical waveforms, such as digital pulsatile chemical waveforms with a frequency higher than 10 Hz and analog chemical waveforms with a frequency higher than 0.2 Hz. The shape, frequency, amplitude, and duty cycle of the waveforms could be also conveniently modulated. To demonstrate the capability of μCFG of probing fast biological processes and elucidate signal transduction pathways in complex signaling networks, a variety of temporal responses of Ca^{2+} signaling to ATP-induced activation of the P_2Y receptor, a prototypical G-protein coupled receptor (GPCR), were investigated in live cells by precisely and dynamically controlling their microenvironment.

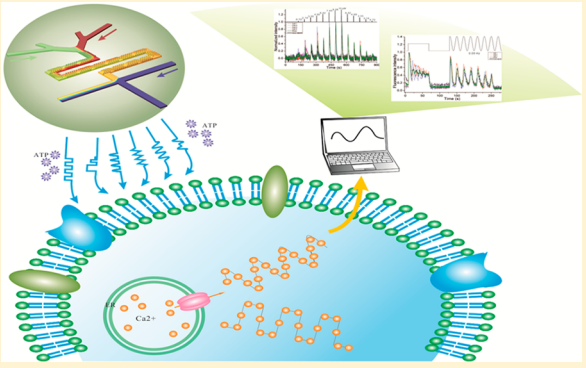

Cellular environments in vivo include complex and temporally varying signals.[1−3] The responses of cells to extracellular microenvironments are also highly dynamic in time and space.[4−8] Among them, G-protein-coupled receptors (GPCRs), such as P2Y receptors, mediate signaling networks that regulate a variety of critical physiological dynamic physiological processes.[9,10] Reconstructing or simulating the physiological environment of the cell in vitro with high spatial and temporal fidelity and imaging of intracellular dynamics in live-cell simultaneously may provide unprecedented insight into the underlying mechanisms of dynamic intercellular signaling networks.

Multiple approaches have used to mimic the complex dynamic environment of cells in vitro, such as photolysis, U-tubes, and perfusion pipettes. Despite their ability to realize solution exchange around single cells, or even cell fragments, use of these technologies to realize a complex, rapid, and well-controlled dynamic exposure have been limited by a lack of precision, poor time resolution, or an inability to flexibly switch solution concentration. Alternatively, emerging microfluidic technologies offer new opportunities to overcome some of these challenges to study cellular signaling dynamics with the aid of the laminar effect on the microscale, and the excellent fluid handling capability of on-chip valves or off-chip components.[11−17] Initial advances in cell-based microdevices focused on the generation of spatial chemical gradients;[18] however, more recently, efforts are being directed to control temporal aspects of stimuli, namely dynamically varying chemical waveforms. Currently, many methods can generate well-tuned time-dependent chemical signals to biological systems, such as scanning output gradients using a moving probe,[19] interface shifting in laminar coflow,[20−23] dynamic gating,[24−28] on- and off-chip valves, acoustic waves,[29] and reconfigurable networks.[30−32] According to the relationship between these chemical signals and time, these methods can be categorized as digital chemical waveforms (i.e., binary/pulsatile switching) or analog chemical waveforms (i.e., continuous manipulation of the amplitude and/or frequency). Despite the rapid evolution of the above-mentioned technologies, to date, there are few methods to realize dynamic digital and analog chemical waveforms simultaneously with high temporal resolution on a single microfluidic chip.

Previously, our group has developed a hydrodynamic gating technique to generate dynamic digital pulsatile chemical signals,[24] but that was limited to only create frequency controllable impulse square waves of uniform amplitude.

Received: May 23, 2017
Accepted: August 9, 2017
Published: August 9, 2017

DOI: 10.1021/acs.analchem.7b01967
Anal. Chem. 2017, 89, 9209−9217

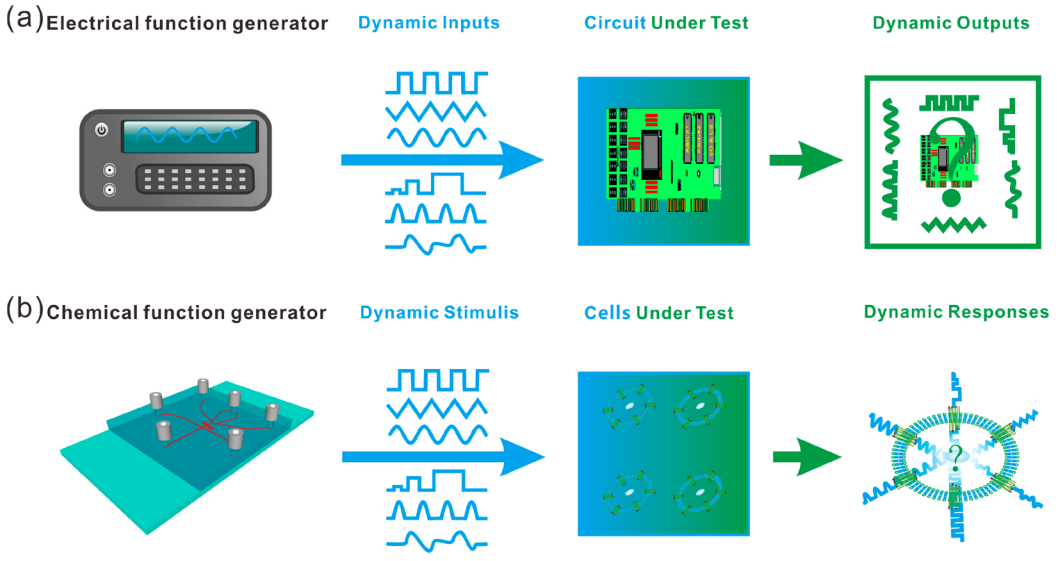

Figure 1. (a) The schematic diagram of an electrical function generator for circuit evaluation and (b) the schematic diagram of a chemical generator for probing dynamic cell signaling based on an integrated microfluidic chip.

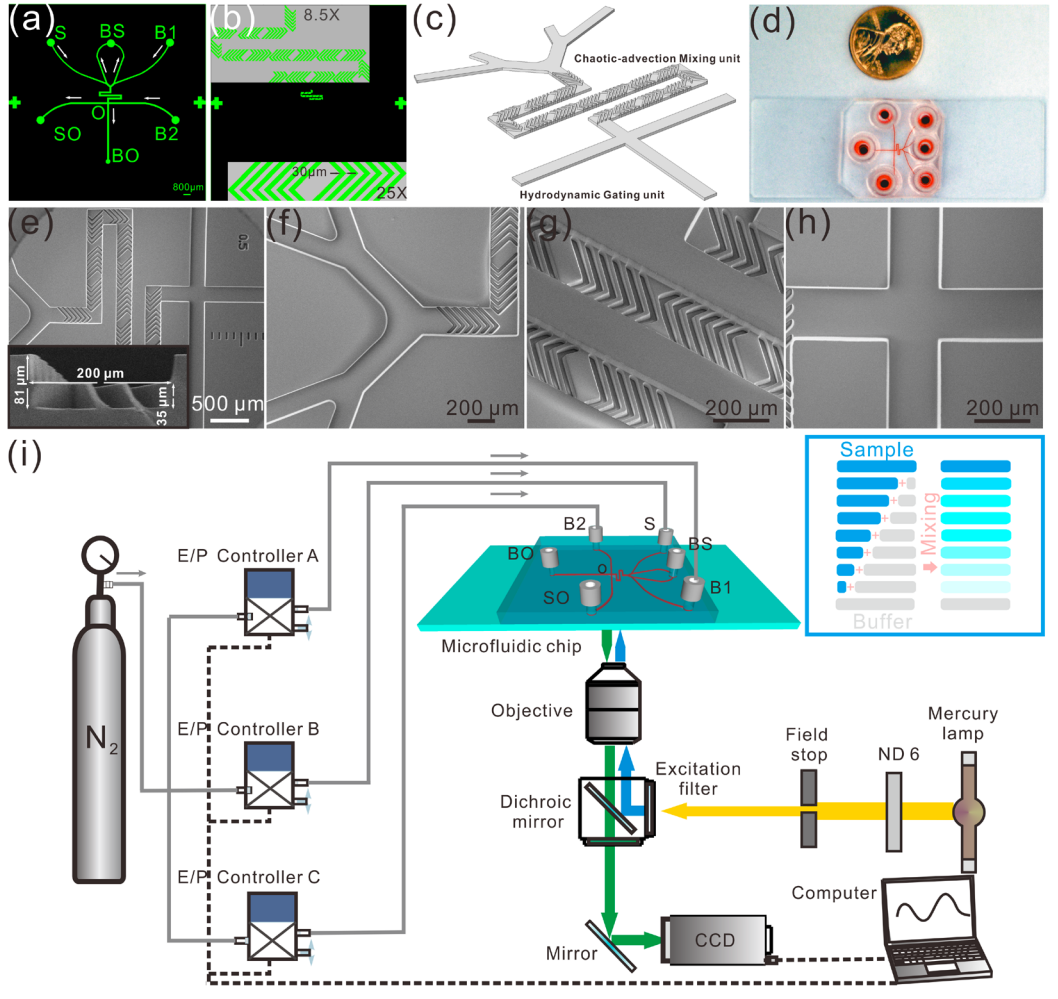

Figure 2. Schematic representations of the microchip design and experimental setup. (a) A mask of the first layer of the microfluidic chip, (b) A mask of the second layer of the microfluidic chip, inset displayed the enlarged pattern in the center of (b), (c) a three-dimensional view of the microfluidic chip, (d) size comparison between a fabricated device and a one-cent coin: the microchannels are visualized by filling them with red food coloring, (e–h) a series of SEM image of the multilayer microchip, (i) schematic diagram of experimental setup: color lines with arrowheads indicate the light path. The dashed lines represent electrical connections. The light gray lines indicate pneumatic connections. Inset displays a schematic diagram of the different mixing results of sample and buffer.

DOI: 10.1021/acs.analchem.7b01967
Anal. Chem. 2017, 89, 9209–9217

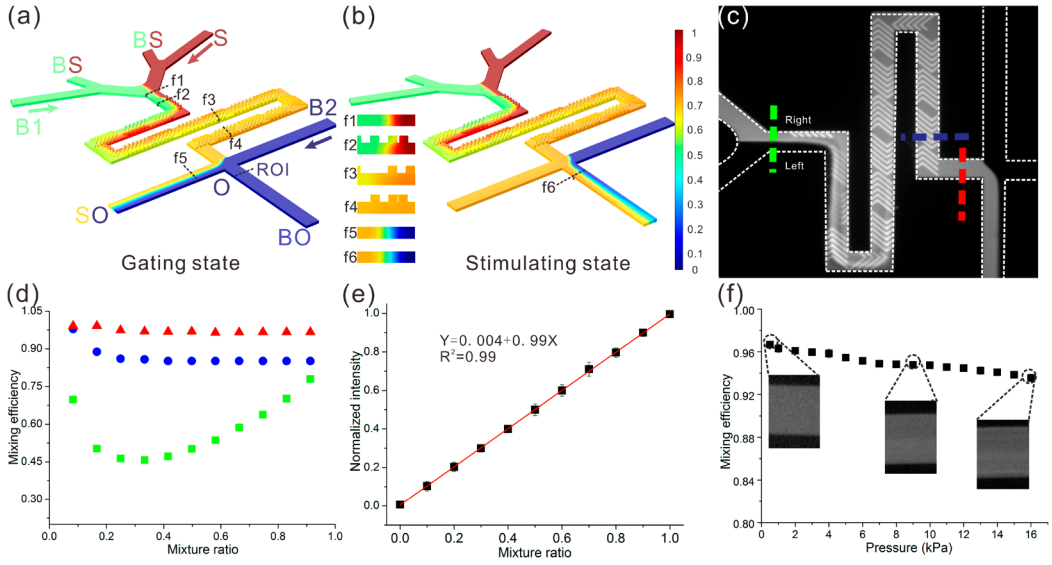

Figure 3. System evaluation. (a, b) Simulation result of the microfluidic chemical function generator of concentration profile in the gating state (a) and the stimulating state (b), inset displays the concentration profile of cross sections marked in (a, b), (c) a typical fluorescence visualization result of the mixing of sample and buffer, and (d) mixing efficiency at different positions for the different mixture ratios: red, blue, and green symbols indicate the mixing efficiency at corresponding position in (c). (e) The normalized fluorescence intensity at different mixture ratios and (f) mixing efficiency at different total pressures of inlet S and B1. The three insets show typical mixed results at three different total pressures.

Inspired by the electrical function generator originally applied in the development and test of electronic equipment (Figure 1a), here we proposed a microfluidic chemical function generator (μCFG) for probing cell dynamic signaling (Figure 1b). It can realize more complex dynamic digital and analog chemical waveforms simultaneously. To achieve a variety of chemical waveforms, the μCFG incorporated a hydrodynamic gating module and a chaotic advection mixing module (Figure 2c), which was able to realize digital pulsatile chemical waveforms of frequency higher than 10 Hz, and analog chemical waveforms of frequency higher than 0.2 Hz. In addition, the shape, frequency, amplitude, and duty cycle of the waveforms could be also conveniently modulated.

EXPERIMENTAL SECTION

Chip Design and Fabrication. We designed a two-layer chip with a hydrodynamic gating unit and a chaotic advection mixing unit in which S, B1, B2, SO, BO, and BS correspond to the sample inlet, buffer inlet 1, buffer inlet 2, sample outlet, buffer outlet and buffer-sample outlet, respectively (Figure 2a). Fabrication details of the microchip are shown in Figure S1 of the Supporting Information, SI, and follow well-established standard rapid prototyping methods. Briefly, negative photoresist SU-8 (GM1070, Gersteltec Sarl, Switzerland) was photolithographically patterned on a silicon wafer to create a master with a two-layer feature.[33] The first SU-8 feature formed the main microfluidic channel with a height of ~45 μm and a width of 200 μm (Figure 2a, e) and the second layer formed a herringbone structure with a height of 35 μm and a width of 30 μm for a single herringbone (Figure 2b). The master was then used as a mold, on which polydimethylsiloxane (PDMS) prepolymer was mixed with its cross-linker at a 10:1 weight ratio before being poured, degassed, casted, and finally put in a conventional oven at 65 °C for 4 h. The cured PDMS replica was removed from the mold and then irreversibly bonded to a glass substrate with a brief plasma treatment. Short glass tubes were attached to punched entrances of each channel to form the final device (Figure 2d). Detailed description of materials and reagents, cell maintenance and culture on microchip, and calcium imaging are provided in the SI.

Apparatus. A schematic drawing of the system setup is shown in Figure 2i. The system contains a microfluidic chip, a custom-built multichannel pressure control module, and a LabView-based signal control module. The pressure control module is composed of three independent E/P transducers (T-1001, Bellofram, U.S.A.), which are used to reduce supply pressures (compressed nitrogen cylinder) to a regulated output pressure directly proportional to a three-wire voltage input with 0.1% accuracy. A home-written LabVIEW (National Instruments, U.S.A.) electrical function generator program was designed to output real-time voltage via a controller card (NI-USB 9263, National Instruments, U.S.A.), which can regulate the pressure control module. The regulated pressure control module can adjust the mixing ratio of sample and buffer (inset in Figure 2i), which could realize automatic dynamic chemical signals with modulated form, frequency, amplitude, and duty cycle.

Experiments were carried out on an inverted fluorescence microscope (IX71, Olympus, Japan) with a CCD camera (Evolve 512, photometrics, U.S.A.) for image acquisition. The light from a mercury lamp (USH1030L, Olympus) was filtered by a 460−490 nm band-pass excitation filter, reflected off a 505 nm dichroic mirror and focused on the target area through a 60× objective (NA 0.7) or a 40× objective (NA 0.6). The emitted fluorescence was collected through the same objective, filtered using a 510 nm highpass filter, and finally detected by the CCD camera. Temperature was maintained at 37 °C using a hot plate (Olympus, Japan) during the experiments. Finally, acquired images were further analyzed using software Image Pro Plus 6.0 and Origin 7.5.

Operation Mechanism. A schematic diagram of μCFG is shown in Figure 3a, b. By gradually adjusting the pressures between S and B1, a different mixture ratio of sample and buffer was generated accordingly in the chaotic advection mixing channel. By controlling the pressures of nitrogen gas on S, B1,

DOI: 10.1021/acs.analchem.7b01967
Anal. Chem. 2017, 89, 9209−9217

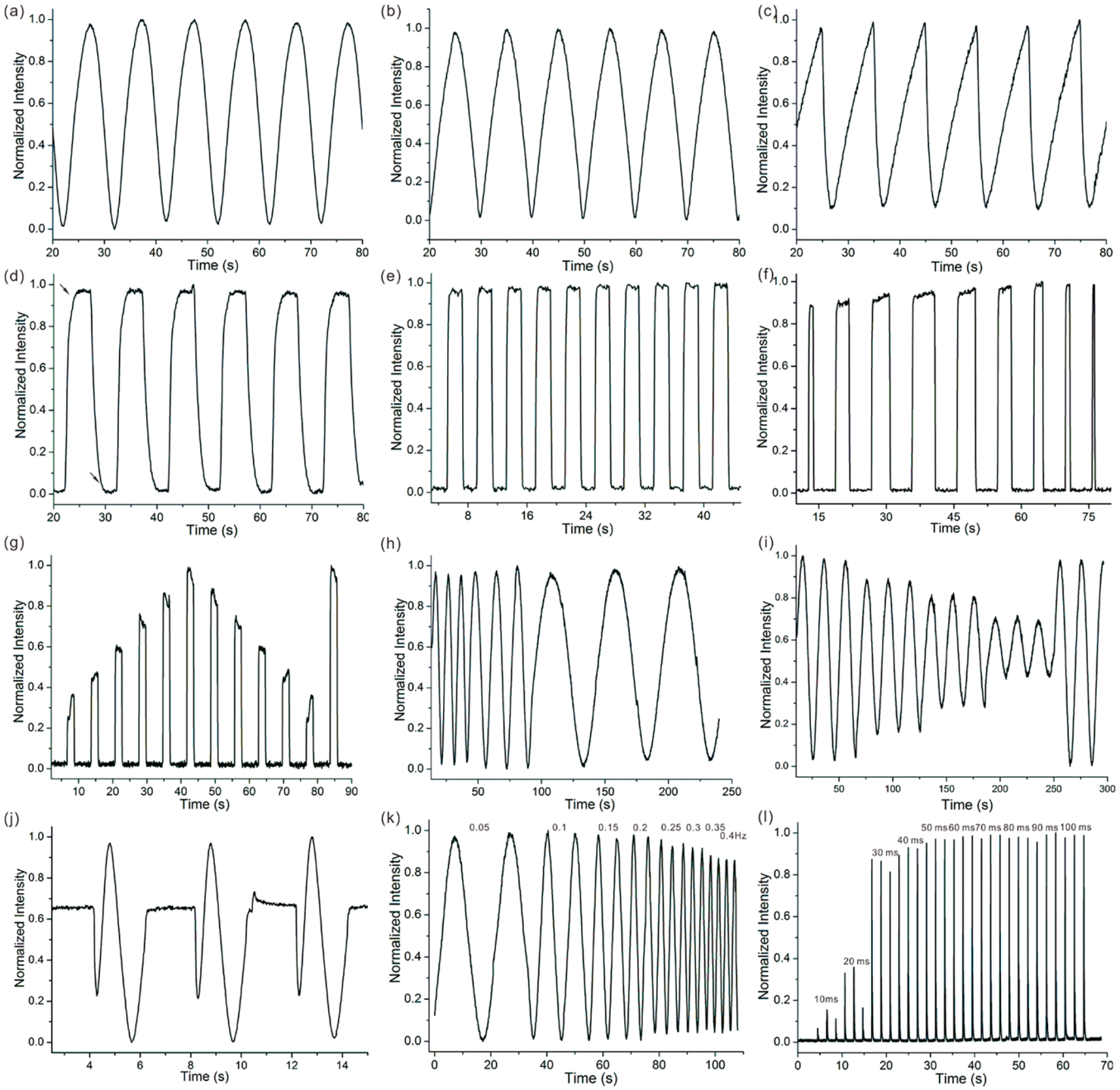

Figure 4. Various waveforms generated by the μCFG. (a) Sinusoidal waveform, (b) triangular waveform, (c) sawtooth waveform, (d) square waveform generated by native system, arrows highlight the slow response in square waveform, (e) square waveform generated by hydrodynamic gating, (f) square waveform with different injection times, (g) square waveform with different amplitudes and the same injection time, (h) sinusoidal waveform with different frequency and the same amplitude, (i) sinusoidal waveform with different amplitude and the same frequency, (j) arbitrary waveforms, (k) sinusoidal waveform of a continuous changing frequency from 0.05 to 0.4 Hz, and (l) square waveforms of a continuously changing injecting time from 10 to 100 ms with a constant relaxation time of 2 s.

and B2, a gating state was formed at the intersection of the microchannel (Figure 3a) and buffer B2 was directed to target cells located on the stimulation channel O−BO. By changing the pressure on B2, it was possible to switch the states between the gating state and the stimulating state. In stimulating state, the output of the mixer was directed to the stimulation channel O−BO to stimulate the target cells (Figure 3b). In addition, due to the combination of hydrodynamic gating, cells located in the stimulation channel could not be stimulated at the beginning of the experiment.

RESULTS AND DISCUSSION

System Evaluation. Operation of the μCFG was performed by carefully adjusting the ratio of pressures upon each entrance. To validate the feasibility of the proposed method, the flow profiles and mass transport in the device were characterized using both numerical simulations and flow visualization experiments. Three-dimensional numerical simulation was conducted using Comsol Multiphysics (COMSOL AB, Sweden) based on the finite element method. The flow patterns and the solution exchange of samples were

DOI: 10.1021/acs.analchem.7b01967
Anal. Chem. 2017, 89, 9209−9217

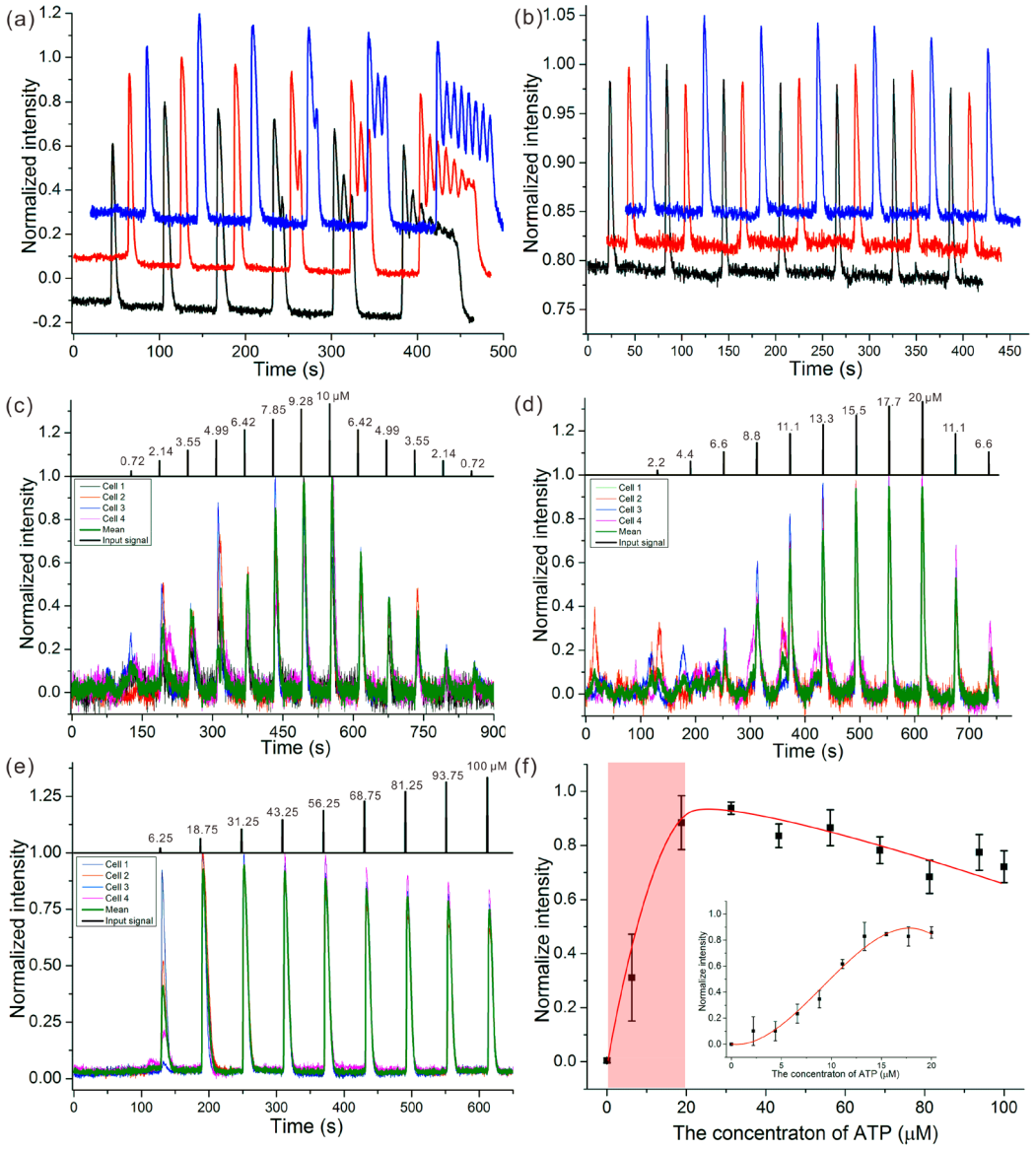

Figure 5. Intracellular dynamics upon pulsatile stimulation. (a) Waterfall graph of single cells responses to repeated injections of 10 μM ATP with increasing injection times (500 ms, 2, 5, 10, 20, and 60 s) and a constant relaxation time of 60 s; (b) waterfall graph of single cells responses to repeated injections of 10 μM ATP with an injection time of 500 ms and a relaxation time of 60 s; (c–e) single cells response to repeated injections of different concentration of ATP with a constant injection time of 500 ms and a constant relaxation time of 60 s, colorful fine line was calcium response of single cell, the green thick line represents the average calcium response; and (f) a dose–response curve of the concentration of ATP from 0 to 100 μM, an enlarged dose–response curve of the area indicated by the red box.

characterized by the steady-state incompressible Navier–Stokes equation and the convective-diffusion equation. The properties of the simulated fluid were set as follows: density of pure water, 0.997×10^3 kg·m^{-3}; viscosity of pure water, 0.895×10^{-3} Pa·s; and the diffusivity of fluorescein solution, 500 μm^2 s^{-1}. The criterion for convergence was for the increment in each variable to be below 1×10^{-5}. The typical simulation results of concentration distribution are shown in Figure 3a, b, and the pressures applied on S, B1, and B2 were set as 1.0, 1.0, and 0.8 kPa for the gating state and 1.0, 1.0, and 0.3 kPa for the stimulating state, respectively. The results showed that the two solutions achieved complete mixing after flowing through the herringbone structure (inset in Figure 3b).

To examine the mixing performance in the fabricated microfluidic chip, fluorescein solution at a concentration of 1×10^{-5} M was introduced into Reservoir S, and buffer solution was added to Reservoirs B1 and B2. After applying the same pressures in the numerical simulations, the observed flow patterns were similar to those from the simulations (Figure 3c), indicating agreement between the experimental results and the numerical simulations. By gradually increasing the pressure on S and decreasing the pressure on B1, the interface shifted from right to left in the chaotic advection mixing channel. Once the interface passed the full width of the mixing channel, the mixture ratio was 100% (Figure S2). Once the critical pressures of both inlets were confirmed (pressures on S and B1 at the mixture ratio of 0% and 100%, respectively), the pressure distribution corresponding to the other mixture ratios could be calculated accordingly. Quantification of the fluorescein distribution was separated into two parameters: concentration and uniformity, measured as the regional mean fluorescence

DOI: 10.1021/acs.analchem.7b01967
Anal. Chem. 2017, 89, 9209–9217

intensity and the mixing efficiency (C_m), respectively.[34] Here C_m was calculated by the following eq 1:

$$C_m = 1 - \frac{\sqrt{\sum (X_i - \bar{X})^2 / N}}{\bar{X}} \quad (1)$$

where X_i was the fluorescence intensity of each point in region of interest, N was the total number of points, and $\bar{X}$ was the average intensity of all of the points. To simplify the calculation, X_i was calculated as each point in the cross line indicated in Figure 3c. The value of C_m ranged from a minimum of 0 to a maximum of 1. A larger C_m value indicated better mixing efficiency, and a C_m equal or greater than 0.9 suggested complete mixing. For quantitative evaluation of the mixing performance, the mixing efficiencies of three given positions were calculated (Figure 3c). Obviously, mixing was complete at the position of the red dotted line at any mixture ratio (Figure 3d), indicating that this chip was able to generate various chemical waveforms. As shown in Figure 3e, the fluorescence intensity of mixed solution increased linearly with the increasing mixture ratio of fluorescein and buffer solution (R^2 = 0.99, n = 3). When the total pressures on S and B1 increased from 1 to 16 kPa, all mixing efficiencies were above 0.9 (Figure 3f), indicating completed mixing under those conditions. In consideration of shear stress, the total pressure of inlet S and B1 was set to 2 kPa, and the pressure of B2 was set to 0.8 kPa on the gating state and 0.3 kPa on the stimulating state, respectively.

Generation of Various Chemical Waveforms. To demonstrate the functionality of the proposed μCFG, varieties of chemical waveforms were generated. Fluorescein solution at a concentration of 1×10^{-5} M was added to inlet S as a stimulant solution, and buffer solution was added into inlet B1 and B2. The chip was then loaded on the platform to detect and record the fluorescence signal (total pressure of inlet S and B1 was 2 kPa). The region of interest (ROI, Figure 3a) for the output waveforms was chosen as ∼300 μm downstream of the intersection O in the channel O−BO. As shown in Figure 4a−d, classical chemical waveforms were generated with sinusoidal, triangular, sawtooth, and square profiles. Statistically, the relative standard deviations of the peak height and baseline were all less than 1%, indicating an outstanding stability and repeatability for the μCFG. We noted, however, that the temporal resolution of modulation square waveforms was limited by the slow response of the pressure control system (Figure 4d, approximately second time-scale). Since a rapid instantaneous stimulation was critical to reduce desensitization of the cell surface receptor, a hydrodynamic gating unit was integrated at the downstream channel to improve the temporal resolution. The downstream hydrodynamic gating combined with the upstream chaotic mixing could rapidly generate square or digital waveforms (Figure 4e) and even their derivative waveforms (Figure 4f, g) with a high temporal resolution of less than 50 ms. Furthermore, the μCFG was able to generate sinusoidal waveforms with adjustable frequency such as 0.05, 0.02, and 0.01 Hz (Figure 4h), and with adjustable amplitude such as from 0% to 100%, 15% to 85%, 25% to 80%, 35% to 65%, and 0% to 100%, where 0% and 100% are the concentrations of the buffer and the sample, respectively (Figure 4i,), and even generate an arbitrary waveform (Figure 4j). To further verify the limits of the time response of μCFG, sinusoidal waveforms of a continuous changing frequency from 0.05 to 0.4 Hz and square or digital waveforms of a continuous changing injecting time from 10 to 100 ms were generated. As shown in Figure 4k, l, the amplitude of the sinusoidal waveforms fell off at frequencies higher than 0.2 Hz, and the amplitude of digital waveforms did not reach a plateau when the injecting time was faster than 50 ms (the corresponding frequency was 10 Hz). The observed limits of the time responses indicated high time resolution of proposed μCFG.

Cells Dynamics upon Pulsatile Stimulation. Among many types of intracellular dynamic signaling pathways, signaling of Ca^{2+}, a second messenger, is crucial in regulation of all kinds of physiological activities in organisms, ranging from transient responses to long-term responses. Because μCFG was able to generate various waveforms with high precision, we next investigated dynamic Ca^{2+} responses when cells were exposed to a wide range of temporal ATP patterns. First, 10 μM ATP with increasing durations from 500 ms to 60 s were consecutively applied to the same single cells. Calcium spikes that evolved from single peak to multiple peaks were observed (Figure 5a). For example, less than 2s of ATP stimulation induced one peak but six to eight peaks were observed when the same cells were exposed to ATP for 60 s. Since cellular signaling can be encoded not only by the frequency, amplitude, and duration, but also by the number of calcium spikes, the proposed μCFG can provided an alternative way to encode intracellular signaling.

It has been reported that sample introduction in a millisecond pulsatile manner with a fixed relaxation time could minimize the desensitization of receptors without compromising functionality.[24] In Figure 5b we show representative responses from three independent cells through repeated injections of 10 μM ATP with an injection time of 500 ms and a relaxation time of 60 s. Relatively stable calcium spikes were also revealed, suggesting minimal receptor desensitization. Our previous work showed that the amplitude of four Ca^{2+} spikes were maintained at a similar level with 20 μM pulses of ATP with increasing durations of 50 ms, 100 ms, 1 s, and 10 s, indicating that the amplitude of cellular responses to ATP are dependent upon the concentration of ATP.[24] In addition, dynamic variation of the concentration of ATP was easily achieved by the μCFG (Figure 4g). On the basis of the above points, the dose−response curve of ATP was obtained by instantaneous and consecutive pulsing of the same single cell with different ATP concentrations. After introducing 10 μM ATP solution into inlet S and the buffer solution into inlet B1 and B2, different ATP concentrations were produced by serial dilution of 10 μM ATP. As shown in Figure 5c, the amplitude of calcium spikes increased gradually with the increasing ATP concentration. To further verify whether this consecutive ATP pulsing could induce desensitization, additional ATP stimulations were performed. Obviously, almost the same amplitudes were obtained at the same ATP concentration, which indicated that there was no significant influence on its functionality. Higher gradient concentrations of ATP were also tested, in which calcium responses also increased with increasing ATP concentration, but reached saturation at 15.5 μM ATP (Figure 5d). Furthermore, use of a stock solution of ATP of 100 μM caused the amplitude of calcium spikes increasing and reaching plateau quickly, then diminishing gradually over time (Figure 5e). A possible explanation of this phenomenon was that a very high concentration of ATP could cause the desensitization of cell receptors. A dose−response curve of calcium responses to 0−100 μM ATP is displayed in Figure 5f, and responses to 0−20 μM ATP are shown in the

DOI: 10.1021/acs.analchem.7b01967
Anal. Chem. 2017, 89, 9209−9217

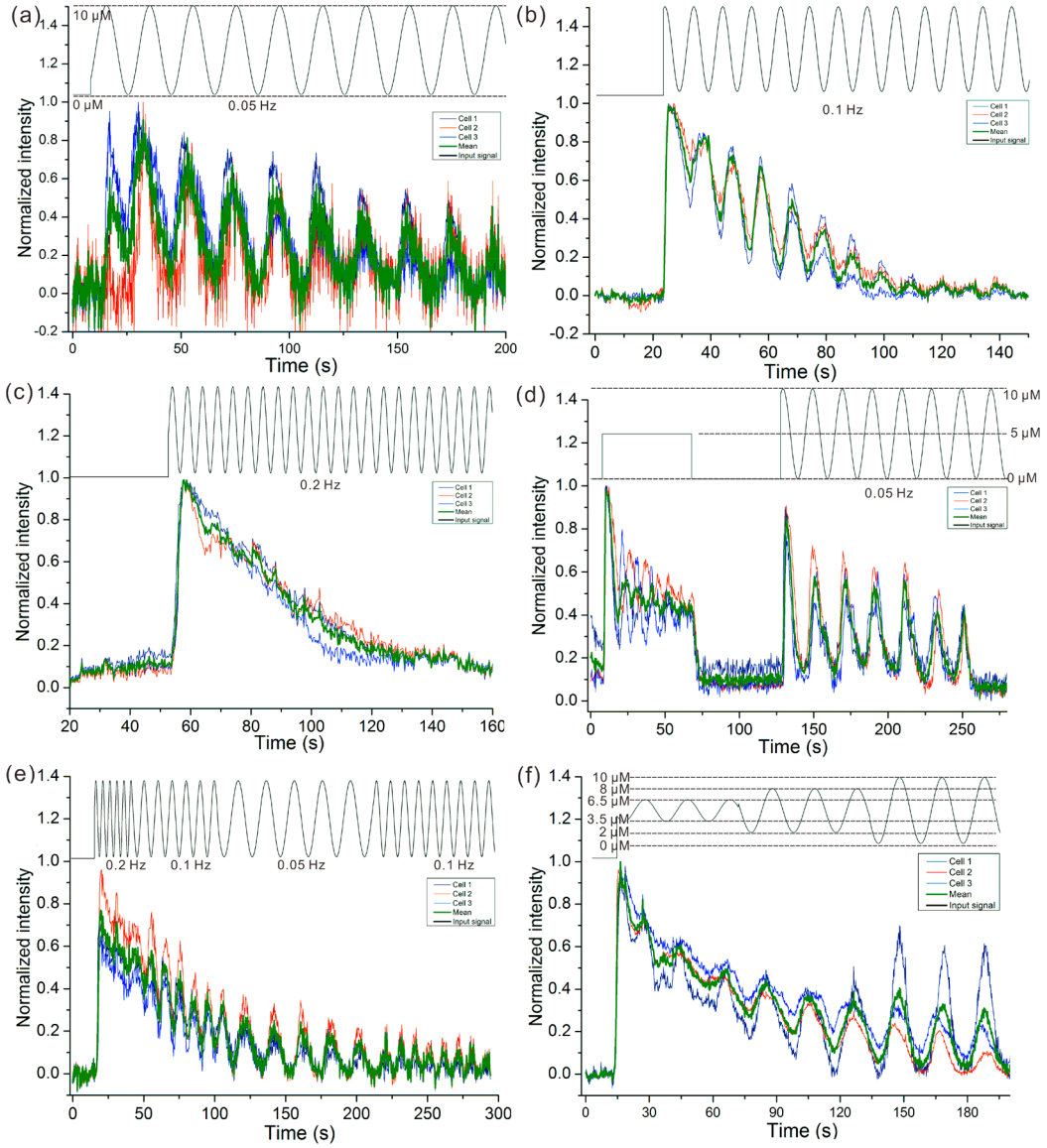

Figure 6. Intracellular dynamic responses upon analogue chemical waveforms stimulation. (a–c) Cell stimulation with sinusoidal waveforms of 0.05, 0.1, and 0.2 Hz, respectively; (d) long-term cell stimulation followed by 0.05 Hz sinusoidal waveforms; (e) cell stimulation with sinusoidal waveforms of continuous varying frequency, and (f) cell stimulation with sine waveforms of different amplitude.

inset map accordingly. In conclusion, compared to the traditional time-consuming and laborious approach using a multiwell plate, the proposed μCFG provides a simple and efficient way to obtain the dose–response curve of drugs.

Probing the Underlying Mechanisms of Cutoff Frequency. Related to pulsing stimulation, another intriguing and yet poorly understood temporal pattern in living systems is the analog periodic chemical stimulus. Different calcium dynamics can affect cell signaling, ultimately leading to changes in cellular function. Nevertheless, despite the prevalence of periodic stimuli, the encoding and decoding of information in these dynamic signals remains poorly understood. To demonstrate the applicability of our device to study dynamic biomolecular processes, we next applied the μCFG to reveal changes in cytosolic calcium in NIH-3T3 cells after exposure to a variety of analog chemical waveforms of ATP. In Figure 6a–c, we show representative results of NIH-3T3 cells exposed to sinusoidal waveforms of 10 μM ATP at 0.05, 0.1, and 0.2 Hz with amplitudes from 0 to 100%. Interestingly, the calcium responses of NIH-3T3 cells were entrained to the external ATP stimulation with high fidelity when the frequency of the signal was not too high (less than 0.1 Hz). Thus, receptor dynamics acted as a low-pass filter, and above a cutoff frequency of 0.2 Hz, there was a low-fidelity response as shown in Figure 6c. In order to elucidate the underlying mechanisms of cutoff frequency, cells were first exposed to a constant concentration of ATP, followed by a sinusoidal ATP waveform. As shown in Figure 6d, stimulation of the NIH-3T3 cells with a constant 10 μM ATP for 60 s induced oscillations with a frequency of about 0.1 Hz. After 60 s relaxation, the same cells were exposed to a frequency of 0.05 Hz sinusoidal waveforms, in which the cells maintained high fidelity. The speculated cutoff frequency may be determined by the inherent oscillation frequency in NIH-3T3 cells. Cells may have different mechanisms to reply to these two kinds of waveforms. The results suggest that we could also use external chemical signals to modulate intracellular signals.

DOI: 10.1021/acs.analchem.7b01967
Anal. Chem. 2017, 89, 9209–9217

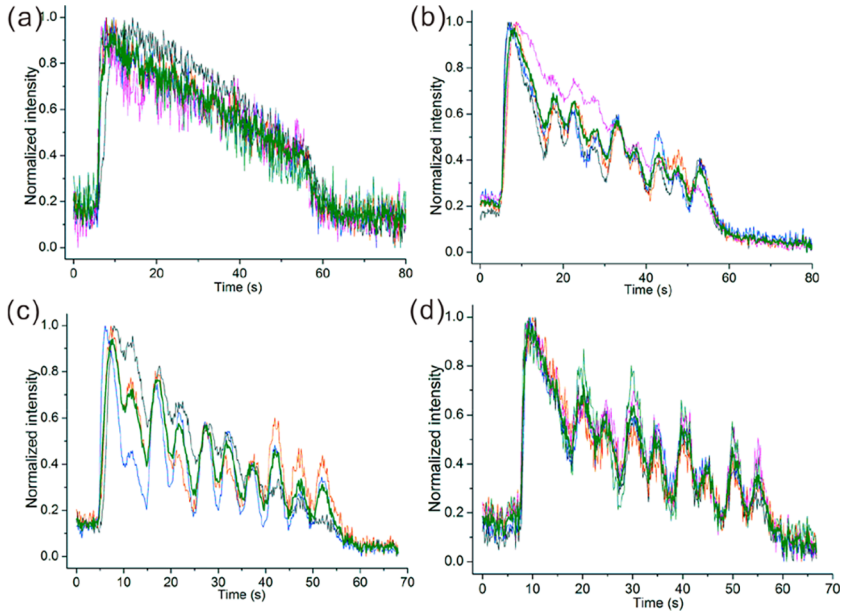

Figure 7. Cell responses upon different ratios of pulsing and relaxation time. (a) Pulsing and relaxation time was set to 2.5 and 2.5 s, respectively; (b) pulsing and relaxation time was set to 1.5 and 3.5 s, respectively; (c) pulsing and relaxation time was set to 1 and 4 s, respectively, and (d) pulsing and relaxation time was set to 0.5 and 4.5 s, respectively.

To further demonstrate the utility of the proposed method, sinusoidal waveforms of 10 μM ATP with different frequencies (0.2, 0.1, and 0.05 Hz) and different amplitude were performed. As in the previous experiment, cells did not respond with high fidelity to initial high frequency stimulation (0.2 Hz), but showed high fidelity under the subsequent lower frequency stimulation (Figure 6e). It was also demonstrated that the responses of calcium signaling to ATP were not only related to its frequency but also its amplitude (Figure 6f).

In order to verify whether the fidelity responses could also exist in pulsing stimulation, we tested dynamic signal responses by changing the pulsing time at a fixed stimulation period of 5 s (corresponding to 0.2 Hz). When the pulsing and relaxation time were both set to 2.5 s, no obvious calcium oscillation was observed (Figure 7a). Interestingly, when the pulsing and relaxation times were set to 1.5 s/3.5 s, 1 s/4, or 0.5 s/4.5 s (Figure 7b–d), calcium oscillation appeared, and its frequency was in line with the input signals of about 0.2 Hz. This indicated that the cutoff frequency could be modulated by an altered ratio of stimulation and relaxation time. This is probably because the effectors in the relevant signal path could partially restore function and can respond to outside input signals at a proper ratio of pulsing time and relaxation time.

CONCLUSIONS

Calcium temporal dynamic features such as frequency, amplitude, and the duration of oscillation, can encode rich intracellular dynamic signaling. By modulating the temporal signal by altering these features, we can investigate how cells respond to temporally varying environments and illustrate the underlying mechanisms of the dynamic properties of cellular signaling networks. We expect the developed platform, in combination with live cell imaging, may facilitate elucidation of signal transduction pathways and allow probing of dynamic cell signaling.

ASSOCIATED CONTENT

Supporting Information

The Supporting Information is available free of charge on the ACS Publications website at DOI: 10.1021/acs.analchem.7b01967.

Materials and reagents (Text S1), cell maintenance and culture on microchip (Text S2), calcium imaging (Text S3), fabrication process of multilayer microchip (Figure S1); and the mixing result at different mixture ratios (Figure S2) (PDF)

AUTHOR INFORMATION

Corresponding Author

*Tel: +86-27-87792203. Fax: +86-27-8779217. E-mail: bfliu@mail.hust.edu.cn (B.-F.L).

ORCID

Peng Chen: 0000-0002-2392-8106

Yiwei Li: 0000-0002-5203-0290

Bi-Feng Liu: 0000-0002-2135-0873

Author Contributions

†These authors contributed equally to this work.

Notes

The authors declare no competing financial interest.

ACKNOWLEDGMENTS

The authors gratefully acknowledge the financial supports from National Natural Science Foundation of China (21475049, 31471257, 21275060 and 31700746) and National Key R&D Program of China (2016YFF0100801).

REFERENCES

(1) Dolmetsch, R. E.; Xu, K. L.; Lewis, R. S. *Nature* **1998**, *392*, 933–936.

(2) Bennett, M. R.; Pang, W. L.; Ostroff, N. A.; Baumgartner, B. L.; Nayak, S.; Tsimring, L. S.; Hasty, J. *Nature* **2008**, *454*, 1119–1122.

(3) Yosef, N.; Regev, A. *Cell* **2011**, *144*, 886–896.

DOI: 10.1021/acs.analchem.7b01967
Anal. Chem. 2017, 89, 9209–9217

(4) Baumgartner, B. L.; Bennett, M. R.; Ferry, M.; Johnson, T. L.; Tsimring, L. S.; Hasty, J. *Proc. Natl. Acad. Sci. U. S. A.* **2011**, *108*, 21087−21092.
(5) Cai, L.; Dalal, C. K.; Elowitz, M. B. *Nature* **2008**, *455*, 485−U416.
(6) Mettetal, J. T.; Muzzey, D.; Gomez-Uribe, C.; van Oudenaarden, A. *Science* **2008**, *319*, 482−484.
(7) Sun, B.; Lembong, J.; Normand, V.; Rogers, M.; Stone, H. A. *Proc. Natl. Acad. Sci. U. S. A.* **2012**, *109*, 7753−7758.
(8) Bennett, M. R.; Hasty, J. *Nat. Rev. Genet.* **2009**, *10*, 628−638.
(9) O'Neill, P. R.; Giri, L.; Karunarathne, W. K. A.; Patel, A. K.; Venkatesh, K. V.; Gautam, N. *Wiley Interdisciplinary Reviews-Systems Biology and Medicine* **2014**, *6*, 115−123.
(10) Zhang, D. D.; Gao, Z. G.; Zhang, K. H.; Kiselev, E.; Crane, S.; Wang, J.; Paoletta, S.; Yi, C. Y.; Ma, L. M.; Zhang, W. R.; Han, G. W.; Liu, H.; Cherezov, V.; Katritch, V.; Jiang, H. L.; Stevens, R. C.; Jacobson, K. A.; Zhao, Q.; Wu, B. L. *Nature* **2015**, *520*, 317−322.
(11) Roper, M. G. *Anal. Chem.* **2016**, *88*, 381−394.
(12) Chingozha, L.; Zhan, M.; Zhu, C.; Lu, H. *Anal. Chem.* **2014**, *86*, 10138−10147.
(13) He, L. Y.; Kniss, A.; San-Miguel, A.; Rouse, T.; Kemp, M. L.; Lu, H. *Lab Chip* **2015**, *15*, 1497−1507.
(14) Kniss-James, A. S.; Rivet, C. A.; Chingozha, L.; Lu, H.; Kemp, M. L. *Integr Biol-Uk* **2017**, *9*, 238−247.
(15) Zhang, X. Y.; Roper, M. G. *Anal. Chem.* **2009**, *81*, 1162−1168.
(16) Takeda, K.; Shao, D. Y.; Adler, M.; Charest, P. G.; Loomis, W. F.; Levine, H.; Groisman, A.; Rappel, W. J.; Firtel, R. A. *Sci. Signal* **2012**, *5*.
(17) Lee, P. J.; Gaige, T. A.; Hung, P. J. *Lab Chip* **2009**, *9*, 164−166.
(18) Lin, F.; Saadi, W.; Rhee, S. W.; Wang, S. J.; Mittal, S.; Jeon, N. L. *Lab Chip* **2004**, *4*, 164−167.
(19) Olofsson, J.; Bridle, H.; Sinclair, J.; Granfeldt, D.; Sahlin, E.; Orwar, O. *Proc. Natl. Acad. Sci. U. S. A.* **2005**, *102*, 8097−8102.
(20) Jovic, A.; Wade, S. M.; Miyawaki, A.; Neubig, R. R.; Linderman, J. J.; Takayama, S. *Mol. BioSyst.* **2011**, *7*, 2238−2244.
(21) Dhumpa, R.; Truong, T. M.; Wang, X.; Roper, M. G. *Integr Biol-Uk* **2015**, *7*, 1061−1067.
(22) King, K. R.; Wang, S.; Jayaraman, A.; Yarmush, M. L.; Toner, M. *Lab Chip* **2008**, *8*, 107−116.
(23) Yi, L.; Wang, X.; Dhumpa, R.; Schrell, A. M.; Mukhitov, N.; Roper, M. G. *Lab Chip* **2015**, *15*, 823−832.
(24) Sun, J.; Chen, P.; Feng, X. J.; Du, W.; Liu, B. F. *Biosens. Bioelectron.* **2011**, *26*, 3413−3419.
(25) Chen, P.; Feng, X.; Sun, J.; Wang, Y.; Du, W.; Liu, B.-F. *Lab Chip* **2010**, *10*, 1472−1475.
(26) Chen, P.; Chen, P.; Feng, X. J.; Du, W.; Liu, B. F. *Anal. Bioanal. Chem.* **2013**, *405*, 307−314.
(27) Chen, P.; Feng, X. J.; Chen, D. J.; Liu, C.; Du, W.; Liu, B. F. *Sens. Actuators, B* **2016**, *234*, 583−592.
(28) Chen, P.; Guo, Y. R.; Wang, J.; Du, W.; Feng, X. J.; Liu, B. F. *Sens. Actuators, B* **2017**, *251*, 112−119.
(29) Ahmed, D.; Muddana, H. S.; Lu, M. Q.; French, J. B.; Ozcelik, A.; Fang, Y.; Butler, P. J.; Benkovic, S. J.; Manz, A.; Huang, T. J. *Anal. Chem.* **2014**, *86*, 11803−11810.
(30) Ainla, A.; Gozen, I.; Orwar, O.; Jesorka, A. *Anal. Chem.* **2009**, *81*, 7858−7858.
(31) Chen, L.; Azizi, F.; Mastrangelo, C. H. *Lab Chip* **2007**, *7*, 850−855.
(32) Azizi, F.; Mastrangelo, C. H. *Lab Chip* **2008**, *8*, 907−912.
(33) Stroock, A. D.; Dertinger, S. K. W.; Ajdari, A.; Mezic, I.; Stone, H. A.; Whitesides, G. M. *Science* **2002**, *295*, 647−651.
(34) Li, Y.; Xu, Y. Z.; Feng, X. J.; Liu, B. F. *Anal. Chem.* **2012**, *84*, 9025−9032.

DOI: 10.1021/acs.analchem.7b01967
Anal. Chem. 2017, 89, 9209−9217